The Crystal Structure of a Complex of Acetylcholinesterase with a Bis-(−)-*nor*-meptazinol Derivative Reveals Disruption of the Catalytic Triad

Aviv Paz,[†,‡,⊥] Qiong Xie,[§,⊥] Harry M. Greenblatt,[†] Wei Fu,[§] Yun Tang,[∥] Israel Silman,[‡] Zhuibai Qiu,[§] and Joel L. Sussman*[,†]

Departments of Structural Biology and Neurobiology, Weizmann Institute of Science, Rehovot 76100, Israel, Department of Medicinal Chemistry, School of Pharmacy, Fudan University, Shanghai 200032, P.R. China, School of Pharmacy, East China University of Science and Technology, Shanghai 200237 P.R. China

Received December 31, 2008

A bis-(−)-*nor*-meptazinol derivative in which the two meptazinol rings are linked by a nonamethylene spacer is a novel acetylcholinesterase inhibitor that inhibits both catalytic activity and Aβ peptide aggregation. The crystal structure of its complex with *Torpedo californica* acetylcholinesterase was determined to 2.7 Å resolution. The ligand spans the active-site gorge, with one *nor*-meptazinol moiety bound at the "anionic" subsite of the active site, disrupting the catalytic triad by forming a hydrogen bond with His440$N^{\varepsilon 2}$, which is hydrogen-bonded to Ser200O^{γ} in the native enzyme. The second *nor*-meptazinol binds at the peripheral "anionic" site at the gorge entrance. A number of GOLD models of the complex, using both native *Tc*AChE and the protein template from the crystal structure of the bis-(−)-*nor*-meptazinol/*Tc*AChE complex, bear higher similarity to the X-ray structure than a previous model obtained using the mouse enzyme structure. These findings may facilitate rational design of new meptazinol-based acetylcholinesterase inhibitors.

Introduction

The enzyme acetylcholinesterase (AChE[a]) terminates impulse transmission at central and peripheral cholinergic synapses by rapid hydrolysis of the neurotransmitter acetylcholine (ACh).[1] It has served as a therapeutic target for the symptomatic treatment of Alzheimer's disease (AD) due to the cholinergic hypothesis, which argues that the cognitive decrements observed in AD patients are associated with impairment of cholinergic transmission.[2,3] The hypothesis thus predicts that inhibition of AChE should prolong the effect of the neurotransmitter ACh, resulting in partial restoration of the cognitive abilities of the patients. As a consequence, the first generation of AD drugs were all acetylcholinesterase inhibitors (AChEIs),[4] and four are currently used extensively, including the synthetic compounds E2020[5] and rivastigmine[6] and the alkaloids galanthamine[7] and (−)-huperzine A.[8]

AChE has been demonstrated to colocalize with the amyloid-β peptide (Aβ) in the brains of AD patients,[9] and has been shown to accelerate the assembly of Aβ to amyloid fibrils.[10] Several ligands that bind at the peripheral anionic site (PAS) of AChE have been shown to retard aggregation.[11,12] Furthermore, a monoclonal antibody directed against the PAS also reversed the effect of AChE on Aβ deposition.[13] In the active-site gorge of AChE, the "anionic" subsite of the active site, also known as the catalytic "anionic" site (CAS), is located at the bottom of the gorge, and the PAS is near its entrance.[14,15] This led to the development of the bivalent ligand approach in which identical or distinct pharmacophores are linked, via an appropriate spacer, to produce a bifunctional drug with enhanced affinity.[16] This, in turn, proved valuable for developing drugs with dual action both in inhibition of catalytic activity and in arresting the AChE-catalyzed assembly of amyloid fibrils (for recent reviews see refs 17 and 18).

Xie and co-workers recently reported the synthesis and characterization of novel bis-(−)-*nor*-meptazinols that inhibit both AChE and butyrylcholinesterase (BChE) as well as retarding Aβ aggregation.[19] The most potent of these compounds

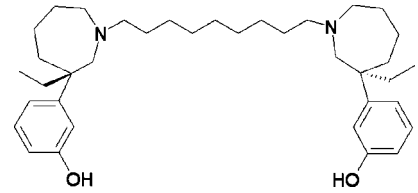

Figure 1. Chemical structure of **5h**.

Table 1. Data Collection and Refinement Statistics

space group	$P3_121$
cell parameters (Å)	$a = 112.17$
	$b = 112.17$
	$c = 137.57$
molecules/asymmetric unit	1
resolution (Å)	40−2.7
total reflections	338424
unique reflections	26746
completeness (%)[a]	99.93% (99.76)
av $I/\sigma(I)$	17.5 (3.55)
R_{merge} (%)[b]	11.7
R (%)[c]	18.5
R_{free} (%)[d]	23.5 (5.2% of data)
rmsd, bond lengths (Å)	0.019
rmsd, bond angles (deg)	2.1
PDB code	2W6C

[a] Values in parentheses relate to the highest resolution shell (2.8−2.7 Å). [b] $R_{merge} = \sum |I - \langle I \rangle| / \sum I$, where I is the observed intensity, and $\langle I \rangle$ is the average intensity obtained from multiple observations of symmetry-related reflections after rejections. [c] $R = \sum ||F_o| - ||F_c|| / \sum |F_o|$, where F_o and F_c are the observed and calculated structure factors, respectively. [d] As defined by ref 38.

* To whom correspondence should be addressed. Phone: 972-8-934-4531. Fax: 972-8-934-4159. E-mail:joel.sussman@weizmann.ac.il.

† Department of Structural Biology, Weizmann Institute of Science.

‡ Department of Neurobiology, Weizmann Institute of Science.

§ Department of Medicinal Chemistry, School of Pharmacy, Fudan University.

∥ School of Pharmacy, East China University of Science and Technology.

⊥ These authors made equal contributions.

[a] Abbreviations: Aβ, amyloid-β peptide; ACh, acetylcholine; AChE, acetylcholinesterase; AChEI, acetylcholinesterase inhibitor; AD, Alzheimer's disease; BuChE, butyrylcholinesterase; CAS, catalytic anionic site; m, mouse; MEP, (−)-meptazinol; PAS, peripheral anionic site; *Tc*, *Torpedo californica*; a, axial; e, equatorial.

10.1021/jm801657v CCC: $40.75
Published on Web 03/27/2009

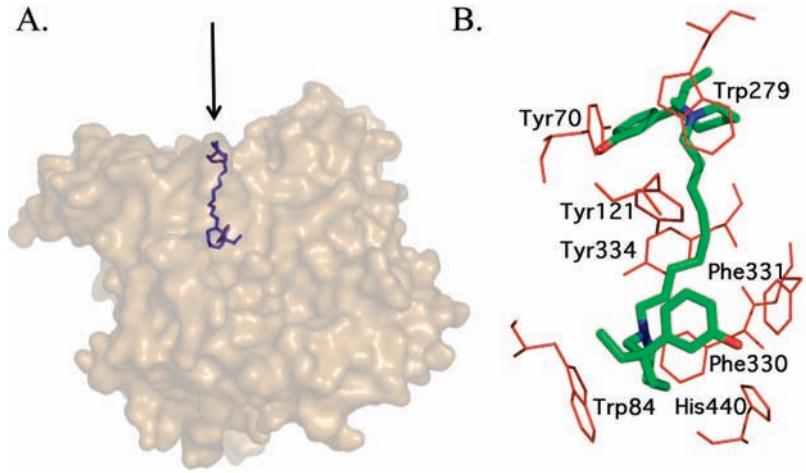

Figure 2. Two representations of the refined structure of the **5h**/*Tc*AChE complex. (A) *Tc*AChE is displayed as a beige space-filling surface and **5h** within the active-site gorge as a magenta stick model. The arrow marks the entrance to the active-site gorge. (B) **5h** shown as a green stick model, and the side chains of selected active-site residues with which it makes contact as red stick models.

was a homodimer with a nine-carbon spacer (**5h**) (Figure 1), which displayed IC_{50} values of 3.9 ± 1.3 and 10.0 ± 3.0 nM toward mouse brain AChE and mouse serum BChE, respectively, and an IC_{50} of 16.6 μM for inhibition of Aβ aggregation. GOLD[20] docking simulations of **5h**, in which the phenyl groups of both MEP moieties were in equatorial orientations with respect to the azapane rings ($e_C e_P$), indicated that **5h** spans the active-site gorge, interacting with both the CAS and PAS of mAChE. The phenyl group of the MEP moiety at the CAS was predicted to make a face-to-face π-stacking interaction with Trp86 (mAChE numbering, Trp84 in *Tc*AChE). The MEP moiety at the PAS was predicted to make cation$-\pi$ and hydrophobic interactions of its seven-membered azepane ring with the indole moiety of Trp286 (*Tc*AChE Trp279). In addition, **5h** was predicted to form two hydrogen bonds at the CAS, one involving interaction of its hydroxyl group with the main chain carbonyl oxygen of His447 (*Tc*AChE His440) and the other involving interaction of its protonated azepane nitrogen with Tyr124O^{ζ} (*Tc*AChE Tyr121).[19]

In the following, we present the crystal structure of a complex of **5h** with *Tc*AChE and new GOLD models based on the *Tc*AChE structure rather than on the mAChE structure. As predicted, **5h** spans the CAS and the PAS. The crystal structure is compared to those obtained by computer docking of **5h** and to the native crystal structures of *Tc*AChE and mAChE.

Materials and Methods

Crystallization and Data Collection. *Tc*AChE was purified essentially as described by Sussman et al.,[21] with the exception of the affinity column elution, which was performed with tetramethylammonium bromide instead of decamethonium bromide. Trigonal crystals of the enzyme[14] were soaked for 20 h at 4 °C in 2 μL of 1 mM **5h**[19] dissolved in the crystallization solution (40% PEG 200 (v/v)/150 mM MES (Sigma-Aldrich), pH 7.4), employing the hanging drop procedure.[22] The crystals were then transferred to cryoprotectant oil and flash frozen in liquid nitrogen.

Data collection was performed at the ESRF in Grenoble, on beamline ID 14−1, at T = 100 K and λ = 0.934 Å. 180 images were taken, at an oscillation angle of 1°, with an exposure time of 6 s. DENZO and SCALEPACK[23] were used to integrate and scale the data. Data were truncated with the CCP4[24] program TRUNCATE,[25] and 5.16% of the reflections were randomly used as test reflections (Table 1).

Structure Determination and Refinement. A model of **5h** was constructed using the GaussView 3.09 program (Gaussian, Carnegie, PA) and converted to a PDB file format using Babel.[26]

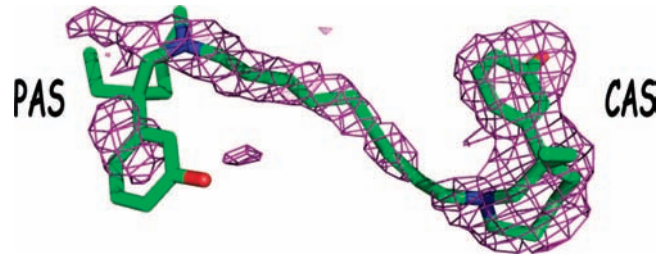

Figure 3. Simulated annealing omit map of the **5h**/*Tc*AChE complex. The MEP moiety at the CAS and the nonamethylene linker display almost complete electron density, whereas the MEP moiety at the PAS does not, suggesting that it assumes multiple conformations. The electron density is contoured at 3σ.

Rigid body refinement in CCP4[24] was based on a previously solved trigonal crystal form of native *Tc*AChE (PDB code 1EA5), excluding water molecules and carbohydrates. Initial $2F_o - F_c$ and $F_o - F_c$ electron density maps were calculated using 40−2.7 Å data, and the initial $F_o - F_c$ map was used, with the aid of the program Coot,[27] to fit **5h** into positive density at the CAS of *Tc*AChE, as well as the spacer, and to add 78 water molecules. Subsequent restrained refinement rounds with overall B-factor refinement were performed and 56 carbohydrate atoms were added until convergence to values of R_{work} = 18.5% and R_{free} = 23.5%. As analyzed by Molprobity,[28] 95.0% of all residues are in favored regions and 99.6% are in allowed regions of the Ramachandran plot, the only outliers being Asp380 and Asn457, which are both glycosylated surface residues. Due to the poor electron density at the PAS observed in the $2F_o - F_c$ map we chose to submit the coordinates of **5h** without the atoms of the MEP moiety within the PAS. In all figures therein, this MEP moiety is shown for descriptive purposes only. Simulated annealing omit maps were constructed using PHENIX.[29]

Molecular Docking. Molecular simulations were performed on an R14000 SGI Fuel workstation with the software package SYBYL 6.9 (Tripos Inc., St. Louis, MO). Standard parameters were used unless otherwise indicated. The crystal structures of both native *Tc*AChE (PDB code 1EA5) and of the **5h**/*Tc*AChE complex were used. Heteroatoms and water molecules in the proteins were removed, and hydrogen atoms were subsequently added.

Three-dimensional structures of **5h** were generated by connecting two (−)-*nor*-MEP units in either equatorial or axial conformations. The equatorial conformation of the (−)-*nor*-MEP unit was retrieved from the crystal structure of MEP.[30] The axial conformation was generated based on earlier NMR studies.[30] Two sp^3 N atoms of **5h** were protonated, and the Gasteiger−Hückel partial charges were

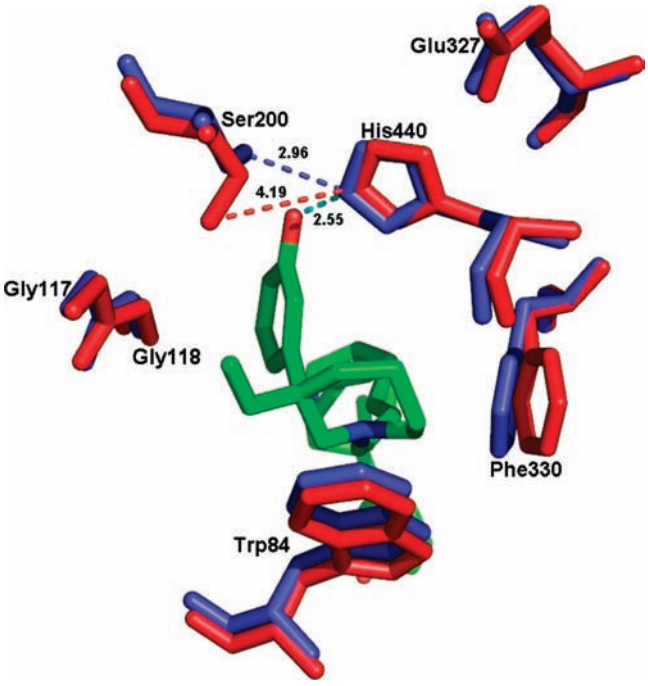

Figure 4. Overlay of the CAS of the **5h**/*Tc*AChE crystal structure on that of native *Tc*AChE. The view is from below the catalytic triad looking up the gorge. The amino acid side chains in the complex are displayed as red sticks and those in the native enzyme as blue sticks. The comparison shows that in the complex the catalytic triad is disrupted due to formation of an H-bond between His440$N^{\varepsilon 2}$ and the phenol oxygen of the MEP moiety (cyan dashed line), with concomitant disruption of its native H-bond with Ser200O^{γ}. As a consequence, the side chain of Ser200 rotates away from His440, widening the distance between His440$N^{\varepsilon 2}$ and Ser200O^{γ} from the native distance of 3.0 Å (blue dashed line) to 4.2 Å (red dashed line). In addition, Phe330 is tilted away from its native position by the seven-membered ring of the MEP moiety.

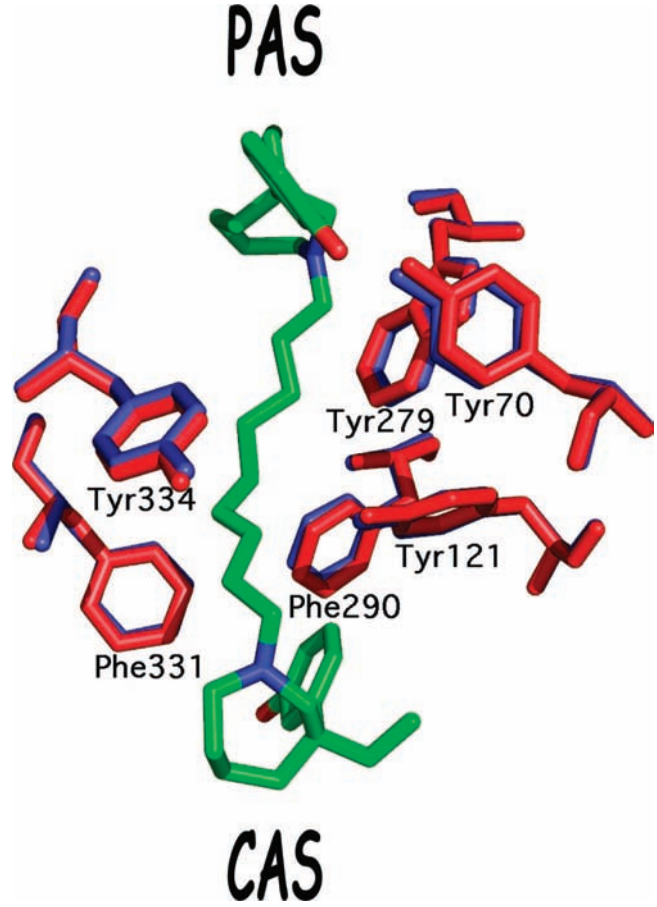

Figure 5. Side view of **5h** and of the residues lining the active-site gorge in the **5h**/*Tc*AChE complex. **5h** is displayed as green sticks, the amino acid side chains in the complex as red sticks, and the corresponding residues in native *Tc*AChE as blue sticks.

assigned. Following this, the ligand was energy minimized in 1000 steps using the Tripos force field.

Molecular docking was carried out using GOLD 3.0 (CCDC, Cambridge, UK, 2005) to generate an ensemble of docked conformations for the ligand. The active site was defined as all atoms within a radius of 25 Å around Tyr121O^{ζ} of *Tc*AChE. This enlarged binding pocket was chosen, as a smaller one might neither accommodate a large bis-ligand nor include both the catalytic and peripheral sites of AChE. Because of the high flexibility of the ligand, which contains many rotatable bonds, 600 genetic algorithm (GA) runs were performed rather than the default of 10. For each GA run, the default GA settings were used, except that early termination was prohibited and pyramidal nitrogen inversion was allowed.

An advanced combination approach of consensus scoring was used to guide the selection of the most reliable conformation(s) from the set of candidate conformations that GOLD generated. All conformations were evaluated with five available scoring functions, including four scoring functions (G_Score, PMF, D_Score, and ChemScore) from the CSCORE module[31] in SYBYL and another stand-alone scoring function, X-SCORE 1.2.1.[32] The "rank-by-rank" strategy reported by Wang et al.[33] was adopted for consensus scoring. The final rank of a certain conformation was calculated by taking the unweighted average of all five scoring functions. The top "re-ranked" solution was chosen as the representative binding mode for the ligand.

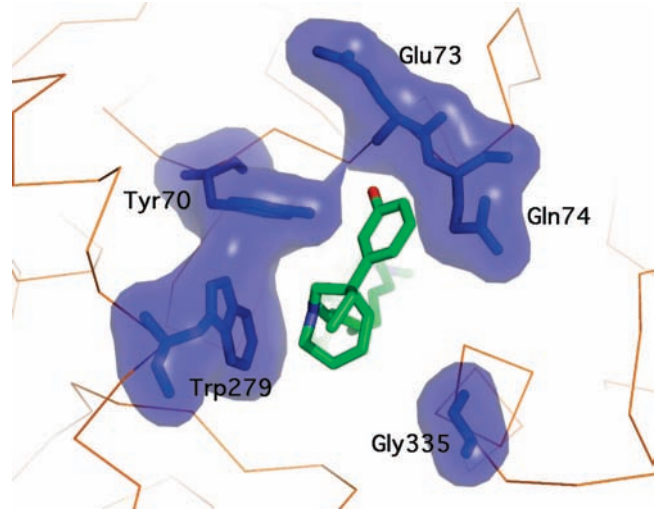

Figure 6. View from above of the entrance to the active-site gorge in the **h5**/*Tc*AChE complex. **5h** is displayed as green sticks, and the backbone of *Tc*AChE is in beige. The side chains of residues lining the entrance to the gorge are displayed as sticks and overlaid with a transparent blue surface.

Results and Discussion

Examination of the crystal structure of the **5h**/*Tc*AChE complex reveals one MEP moiety in the CAS and the other in the PAS, with the nonamethylene spacer that links them snaking along the gorge (Figure 2). The simulated annealing omit map generated for the final refined structure shows full electron density for the MEP moiety at the CAS and for most of the linker, except for a lack of electron density for the second carbon

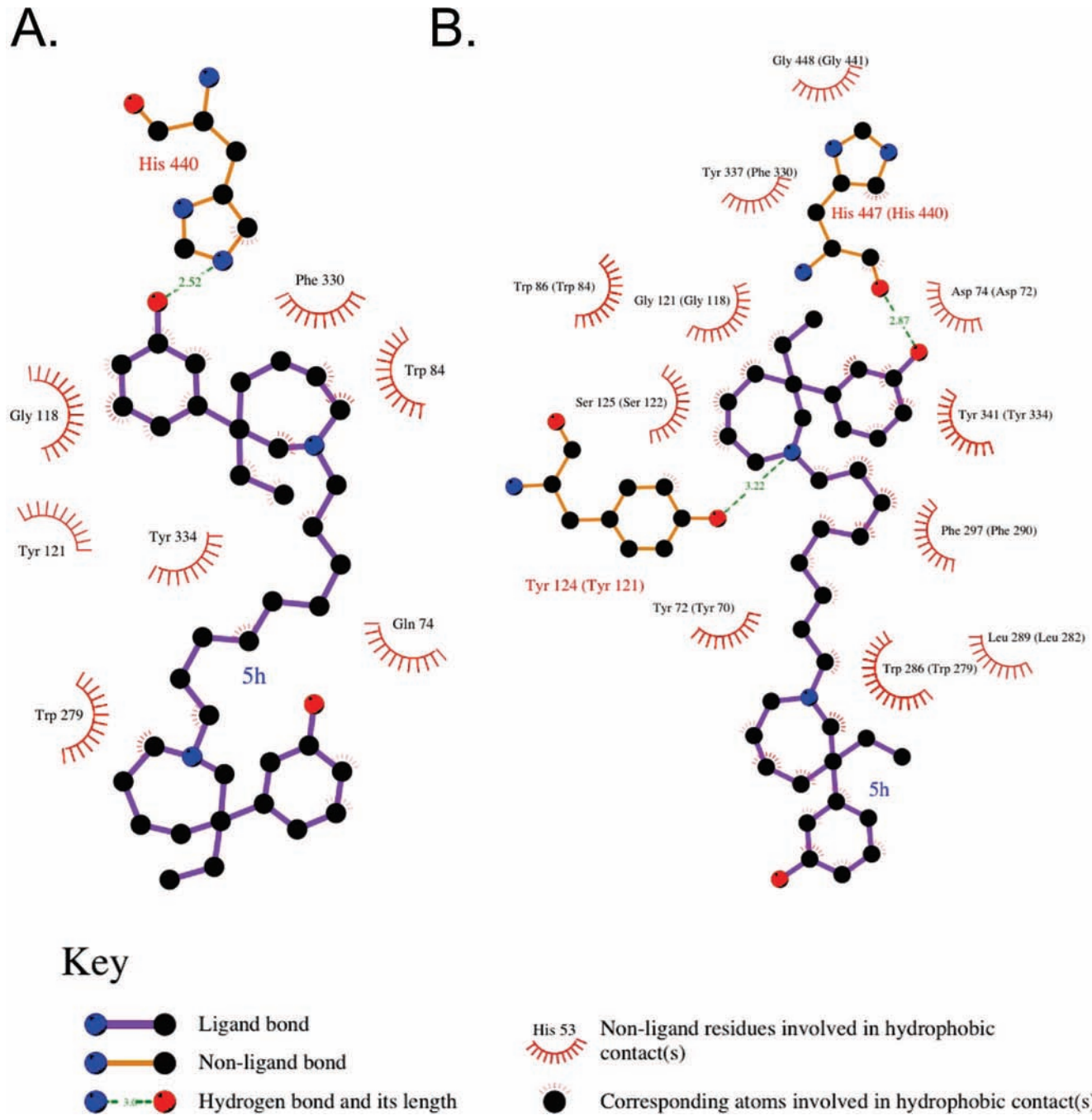

Figure 7. Ligplot representations of interactions of **5h** with AChE. (A) Interactions in the crystal structure of the **5h**/*Tc*AChE complex. (B) Interactions in the model of the **5h**/mAChE complex.[19] In the representation of the model, mAChE numbering is followed by *Tc*AChE numbering in brackets.

Table 2. Scores for the Different Conformations of the CAS and Linker Region of **5h** Modeled by GOLD

template for docking	G_Score	rank	PMF	rank	D_Score	rank	chemscore	rank	X-SCORE	rank	rerank	rmsd[a](Å)
1ea5_aa_027	−233.44	4	−99.89	8	−172.83	5	−39.59	4	6.48	7	5.4	1.19
1ea5_ea_521	−199.81	8	−101.96	7	−170.87	6	−38.45	6	6.51	6	6.2	1.63
1ea5_ee_531	−218.8	7	−107.12	3	−176	4	−38.27	21	6.61	5	5	1.82
2w6c_aa_147	−229.92	5	−103.57	6	−169.67	7	−43.68	11	6.39	8	5.4	1.88
2w6c_ea_220	−240.92	3	−125.63	1	−177.82	2	−37.5	1	6.92	2	3.2	1.15
2w6c_ee_447	−255.25	1	−120.04	2	−179.1	1	−37.66	2	6.97	1	2.4	1.18

[a] The rmsd is calculated for each model in comparison to the crystal structure of **5h**. The PAS MEP moiety was omitted from the rmsd calculations.

of the linker, just above the MEP moiety at the CAS (Figure 3). At the PAS, however, the electron density for the MEP moiety is poorly defined; taken together with the fact that additional positive difference density is observed around it, it seems plausible that the MEP moiety adopts more than one conformation.

At the CAS, the MEP moiety is in an axial orientation and forms contacts with Trp84, Gly117−119, Phe330, and His440

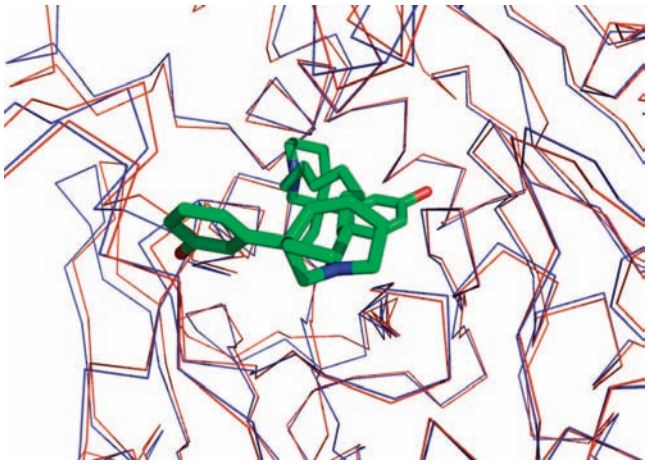

Figure 8. Superposition of the active-site gorge area in the crystal structures of the **5h**/*Tc*AChE complex and of native mAChE looking down the gorge. No significant differences in main chain or side chain conformations are observed between the *Tc*AChE structure (blue) and the mAChE structure (red). Only the main chains are traced for clarity; **5h** is shown in green.

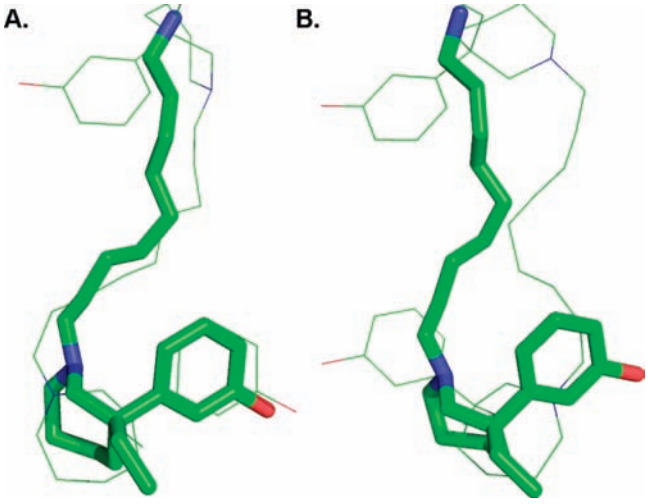

Figure 9. Comparison of the conformation of the MEP moiety in the CAS of the **5h**/*Tc*AChE crystal structure with its conformation in two models obtained by docking to the protein template of the crystal structure (PDB code 2W6C). (A) Superposition of one such model (rmsd = 1.15 Å, rerank = 3.2) shows good agreement between the crystal structure and the model. (B) Superposition of the other model (rmsd = 1.18 Å, rerank = 2.4) on the crystal structure yields a totally incorrect orientation. The crystal structure is displayed as thick sticks and the models as lines.

(Figure 4). Its phenolic oxygen forms a hydrogen bond with His440$N^{\varepsilon 2}$ (2.55 Å), thus disrupting the latter's hydrogen bond with Ser200O^{γ} within the catalytic triad. The χ_1 angle of the freed Ser200 is rotated ~120° relative to its position in the native crystal structure (PDB code 1EA5). As a consequence, the distance between Ser200O^{γ} and His440$N^{\varepsilon 2}$ increases from ~3.0 Å in the native structure to ~4.2 Å. An analogous rupture of the catalytic triad and rotation of Ser200 was observed in the complex of *Tc*AChE with a bis-tacrine inhibitor with a pentamethylene spacer.[34] Phe330 also undergoes a conformational change, relative to the native structure, that involves ~25° and ~33° rotations, respectively, of its χ_1 and χ_2 angles. The residues lining the gorge between the two MEP moieties do not reveal any substantial changes relative to their positions and conformations in native *Tc*AChE (Figure 5).

At the PAS, as already noted, the electron density suggests that the MEP moiety samples more than one conformation. The principal residues surrounding it are Tyr70, Glu73, Gln74, Trp279, and Gly335 (Figure 6), but the conformational heterogeneity precludes assignment of specific interactions. The possibility was considered that the apparent conformational heterogeneity might reflect chemical inhomogeneity, but mass spectrometry of the compound clearly excluded this possibility (not shown).

Ligplot[35] was used to compare the principal ligand−protein interactions of **5h** in the *Tc*AChE crystal structure (Figure 7A) and in the previously published modeled complex with mAChE. In this model, the MEP moieties are both in the equatorial position because this conformation was that found in the small molecule X-ray structure of MEP[30] (Figure 7B).

Superposition of the crystal structures of native mAChE (PDB code 2HA2) and of the **5h**/*Tc*AChE complex (Figure 8) reveals no significant main chain or side chain differences that could provide a basis for the differences between the latter and the model of the **5h**/mAChE complex obtained using GOLD.[19] There is overall similarity in the positioning of the ligand (rmsd = 3.01 Å), with hydrophobic interactions with Trp84, Phe330, and Tyr334 (or the corresponding mAChE residues) appearing in both the crystal structure and the computational model. However, as mentioned above, there are significant differences as well. Thus, in the X-ray structure, His440 is hydrogen-bonded to **5h** through the $N^{\varepsilon 2}$ atom of its imidazole side chain, not through its main-chain carbonyl oxygen, as was suggested by the GOLD model. Furthermore, the crystal structure does not reveal $\pi-\pi$ stacking interactions between Trp84 and the phenyl group of the MEP group bound at the CAS nor hydrogen-bonding of the protonated azepane nitrogen to Tyr121O^{ζ} (Tyr124O^{ζ} in mAChE).

On the basis of the **5h**/*Tc*AChE crystal structure, we decided to carry out additional GOLD simulations, with the same algorithm and parameters that we previously used, in which both MEP moieties in **5h** could adopt either axial or equatorial orientations (aa and ee, respectively) or could adopt mixed orientations (ea and ae) both in the native enzyme (PDB code 1EA5) and in the template of the **5h**/*Tc*AChE complex, devoid of **5h**, waters, and hydrocarbons. This was done to reconcile the observation that there was a difference between the axial orientation of the MEP moiety at the CAS determined by the complex X-ray structure and the equatorial orientations of the ligand used in the GOLD model, while the NMR solution structure of MEP detected both the axial and equatorial conformers.[36] Table 2 lists the conformations and scores obtained (models are available as Supporting Information).

In this modeling study, we found rather than using either *Tc*AChE (1EA5) or mAChE, that in general the best scores were obtained for **5h** modeled inside the empty template of the **5h**/*Tc*AChE complex structure (PDB code 2W6C). When the two best models, 2w6c_ea_220 and 2w6c_ee_447, were superimposed on **5h** from the crystal structure of the complex (Figure 9), it could be seen that the modeled binding mode of the MEP moiety at the CAS was quite similar to that in the crystal structure in the case of 2w6c_ea_220 (Figure 9A), even though their orientations are e_C in the model and a_C in the experimental structure, respectively. However in the second model, 2w6c_ee_447, the CAS MEP moiety assumes a different orientation (Figure 9B). Both models have high ranks (Table 2), exemplifying the difficulty in choosing a *single* model, rather than an ensemble of models, in the absence of a crystal structure of a complex. No comparison of the MEP moieties at the PAS

was made because, as discussed, the electron density there is quite poor, most likely due to local disorder and the rmsd between the **5h** from the crystal structure and the models was calculated only for the CAS MEP, linker region, and the nitrogen of the CAS MEP. Most of the different GOLD models obtained for this complex, using different AChE molecules (apo and holo enzymes, *Tc* and mouse), share an overall similarity but many, in detail, fail to capture the exact nuances of the **5h**−*Tc*AChE interactions.

Since an earlier modeling study of a MEP/*Tc*AChE complex placed the azepane ring in the middle of the gorge with the phenol oriented down the gorge toward the catalytic site,[37] the bivalent MEP derivatives were designed and synthesized with the spacers attached via the azepane rings and not through the oxygen atoms of the phenol groups.[19] The crystal structure of the **5h**/*Tc*AChE complex described here displays a somewhat similar orientation of MEP within the CAS but also reveals high flexibility of the MEP moiety at the PAS. It might, therefore, be worth considering use of another atom on the azepane ring for linkage to the spacer or even synthesizing a molecule in which one MEP would be connected through its phenol group and the other through its azepane ring. These derivatives might have different affinities and specificities for AChE and possibly bind more specifically to the PAS than **5h**. This could provide information as to whether flexible binding of moieties at the PAS might affect the inhibitory effect on Aβ deposition.

Acknowledgment. This work was supported in part by the grants by the Divadol Foundation, the Israel Science Foundation, the Nalvyco Foundation, the Neuman Foundation, the Bruce Rosen Foundation, the Jean and Jula Goldwurm Memorial Foundation, a research grant from Erwin Pearl, the Benoziyo Center for Neuroscience, the European Commission Sixth Framework Research and Technological Development Programme "SPINE2-COMPLEXES" project under contract number LSHG-CT-2006-031220, "Teach-SG" project under contract number ISSG-CT-2007-037198 (I.S. and J.L.S.), and by grants from the National Natural Science Foundation of P.R. China (nos. 30472088 and 30772553) and the Chinese 111 Project grant to ECUST. J.L.S. is the Morton and Gladys Pickman Professor of Structural Biology. We are grateful to Esther Roth and Lilly Toker for the samples of purified *Tc*AChE.

Supporting Information Available: Structures of PDB 2W6C (ZIP): 2w6c_rr6_ee_447.pdb, 2w6c_rr6_ea_220.pdb, 2w6c_rr6_aa_147.pdb, 2w6c_1ea5_ee_531.pdb, 2w6c_1ea5_ea_521.pdb, 2w6c_1ea5_aa_027.pdb. This material is available free of charge via the Internet at http://pubs.acs.org.

References

(1) Rosenberry, T. L. Acetylcholinesterase. *Adv. Enzymol. Relat. Areas Mol. Biol.* **1975**, *43*, 103–218.
(2) Bartus, R. T.; Dean, R. L., III; Beer, B.; Lippa, A. S. The cholinergic hypothesis of geriatric memory dysfunction. *Science* **1982**, *217*, 408–414.
(3) Dunnett, S. B.; Fibiger, H. C. Role of forebrain cholinergic systems in learning and memory: relevance to the cognitive deficits of aging and Alzheimer's dementia. *Prog. Brain Res.* **1993**, *98*, 413–420.
(4) Greenblatt, H. M.; Dvir, H.; Silman, I.; Sussman, J. L. Acetylcholinesterase: a multifaceted target for structure-based drug design of anticholinesterase agents for the treatment of Alzheimer's disease. *J. Mol. Neurosci.* **2003**, *20*, 369–383.
(5) Kawakami, Y.; Inoue, A.; Kawai, T.; Wakita, M.; Sugimoto, H.; Hopfinger, A. J. The rationale for E2020 as a potent acetylcholinesterase inhibitor. *Bioorg. Med. Chem.* **1996**, *4*, 1429–1446.
(6) Enz, A.; Boddeke, H.; Gray, J.; Spiegel, R. Pharmacologic and clinicopharmacologic properties of SDZ ENA 713, a centrally selective acetylcholinesterase inhibitor. *Ann. N.Y. Acad. Sci.* **1991**, *640*, 272–275.
(7) Harvey, A. L. The pharmacology of galanthamine and its analogues. *Pharmacol. Ther.* **1995**, *68*, 113–128.
(8) Zhang, R. W.; Tang, X. C.; Han, Y. Y.; Sang, G. W.; Zhang, Y. D.; Ma, Y. X.; Zhang, C. L.; Yang, R. M. Drug evaluation of huperzine A in the treatment of senile memory disorders. *Acta Pharmacol. Sin.* **1991**, *12*, 250–252.
(9) Alvarez, A.; Bronfman, F.; Perez, C. A.; Vicente, M.; Garrido, J.; Inestrosa, N. C. Acetylcholinesterase, a senile plaque component, affects the fibrillogenesis of amyloid-beta-peptides. *Neurosci. Lett.* **1995**, *201*, 49–52.
(10) Alvarez, A.; Opazo, C.; Alarcon, R.; Garrido, J.; Inestrosa, N. C. Acetylcholinesterase promotes the aggregation of amyloid-beta-peptide fragments by forming a complex with the growing fibrils. *J. Mol. Biol.* **1997**, *272*, 348–361.
(11) Inestrosa, N. C.; Alvarez, A.; Perez, C. A.; Moreno, R. D.; Vicente, M.; Linker, C.; Casanueva, O. I.; Soto, C.; Garrido, J. Acetylcholinesterase accelerates assembly of amyloid-beta-peptides into Alzheimer's fibrils: possible role of the peripheral site of the enzyme. *Neuron* **1996**, *16*, 881–891.
(12) Bartolini, M.; Bertucci, C.; Cavrini, V.; Andrisano, V. beta-Amyloid aggregation induced by human acetylcholinesterase: inhibition studies. *Biochem. Pharmacol.* **2003**, *65*, 407–416.
(13) Reyes, A. E.; Perez, D. R.; Alvarez, A.; Garrido, J.; Gentry, M. K.; Doctor, B. P.; Inestrosa, N. C. A monoclonal antibody against acetylcholinesterase inhibits the formation of amyloid fibrils induced by the enzyme. *Biochem. Biophys. Res. Commun.* **1997**, *232*, 652–655.
(14) Sussman, J. L.; Harel, M.; Frolow, F.; Oefner, C.; Goldman, A.; Toker, L.; Silman, I. Atomic structure of acetylcholinesterase from *Torpedo californica*: a prototypic acetylcholine-binding protein. *Science* **1991**, *253*, 872–879.
(15) Silman, I.; Sussman, J. L. Acetylcholinesterase: "classical" and "nonclassical" functions and pharmacology. *Curr. Opin. Pharmacol.* **2005**, *5*, 293–302.
(16) Pang, Y. P.; Quiram, P.; Jelacic, T.; Hong, F.; Brimijoin, S. Highly potent, selective, and low cost bis-tetrahydroaminacrine inhibitors of acetylcholinesterase. Steps toward novel drugs for treating Alzheimer's disease. *J. Biol. Chem.* **1996**, *271*, 23646–23649.
(17) Du, D. M.; Carlier, P. R. Development of bivalent acetylcholinesterase inhibitors as potential therapeutic drugs for Alzheimer's disease. *Curr. Pharm. Des.* **2004**, *10*, 3141–3156.
(18) Haviv, H.; Wong, D. M.; Silman, I.; Sussman, J. L. Bivalent ligands derived from Huperzine A as acetylcholinesterase inhibitors. *Curr. Top. Med. Chem.* **2007**, *7*, 375–387.
(19) Xie, Q.; Wang, H.; Xia, Z.; Lu, M.; Zhang, W.; Wang, X.; Fu, W.; Tang, Y.; Sheng, W.; Li, W.; Zhou, W.; Zhu, X.; Qiu, Z.; Chen, H. Bis-(−)-*nor*-meptazinols as novel nanomolar cholinesterase inhibitors with high inhibitory potency on amyloid-beta aggregation. *J. Med. Chem.* **2008**, *51*, 2027–2036.
(20) Jones, G.; Willett, P.; Glen, R. C.; Leach, A. R.; Taylor, R. Development and validation of a genetic algorithm for flexible docking. *J. Mol. Biol.* **1997**, *267*, 727–748.
(21) Sussman, J. L.; Harel, M.; Frolow, F.; Varon, L.; Toker, L.; Futerman, A. H.; Silman, I. Purification and crystallization of a dimeric form of acetylcholinesterase from *Torpedo californica* subsequent to solubilization with phosphatidylinositol-specific phospholipase C. *J. Mol. Biol.* **1988**, *203*, 821–823.
(22) McPherson, A. *Preparation and Analysis of Protein Crystals*; John Wiley & Sons: New York, 1982.
(23) Otwinowski, Z.; Minor, W. Processing of X-ray diffraction data collected in oscillation mode. *Methods Enzymol.* **1997**, *276*, 307–326.
(24) CCP4. The CCP4 suite: programs for protein crystallography. *Acta Crystallogr., Sect. D: Biol. Crystallogr.* **1994**, *50*, 760−763.
(25) French, G. S.; Wilson, K. S. On treatment of negative intensity observations. *Acta Crystallogr., Sect. A: Found. Crystallogr.* **1978**, *34*, 517–525.
(26) Walters, P.; Stahl, M., *Babel, version 1.1*; Department of Chemistry, University of Arizona: Tucson, AZ, 1994.
(27) Emsley, P.; Cowtan, K. Coot: Model-Building Tools for Molecular Graphics. *Acta Crystallogr., Sect. D: Biol. Crystallogr.* **2004**, *60*, 2126–2132.
(28) Davis, I. W.; Leaver-Fay, A.; Chen, V. B.; Block, J. N.; Kapral, G. J.; Wang, X.; Murray, L. W.; Arendall, W. B., III; Snoeyink, J.; Richardson, J. S.; Richardson, D. C. MolProbity: all-atom contacts and structure validation for proteins and nucleic acids. *Nucleic Acids Res.* **2007**, *35*, W375–W383.
(29) Adams, P. D.; Grosse-Kunstleve, R. W.; Hung, L. W.; Ioerger, T. R.; McCoy, A. J.; Moriarty, N. W.; Read, R. J.; Sacchettini, J. C.; Sauter, N. K.; Terwilliger, T. C. PHENIX: building new software for automated crystallographic structure determination. *Acta Crystallogr., Sect. D: Biol. Crystallogr.* **2002**, *58*, 1948–1954.
(30) Chen, Y. Studies on the synthesis, resolution and optical isomers of meptazinol. Dissertation. Fudan Univ: Shanghai, 2004; pp 19−28.

(31) Clark, R. D.; Strizhev, A.; Leonard, J. M.; Blake, J. F.; Matthew, J. B. Consensus scoring for ligand/protein interactions. *J. Mol. Graphics. Modell.* **2002**, *20*, 281–295.
(32) Wang, R.; Lai, L.; Wang, S. Further development and validation of empirical scoring functions for structure-based binding affinity prediction. *J. Comput.-Aided Mol. Des.* **2002**, *16*, 11–26.
(33) Wang, R.; Lu, Y.; Wang, S. Comparative evaluation of 11 scoring functions for molecular docking. *J. Med. Chem.* **2003**, *46*, 2287–2303.
(34) Rydberg, E. H.; Brumshtein, B.; Greenblatt, H. M.; Wong, D. M.; Shaya, D.; Williams, L. D.; Carlier, P. R.; Pang, Y. P.; Silman, I.; Sussman, J. L. Complexes of alkylene-linked tacrine dimers with *Torpedo californica* acetylcholinesterase: binding of bis(5)-tacrine produces a dramatic rearrangement in the active-site gorge. *J. Med. Chem.* **2006**, *49*, 5491–5500.
(35) Wallace, A. C.; Laskowski, R. A.; Thornton, J. M. LIGPLOT: a program to generate schematic diagrams of protein−ligand interactions. *Protein Eng.* **1995**, *8*, 127–134.
(36) Li, W.; Wang, X. H.; Lau, C. W.; Tang, Y.; Xie, Q.; Qiu, Z. B. Conformational re-analysis of (+)-meptazinol: an opioid with mixed analgesic pharmacophores. *Acta Pharmacol. Sin.* **2006**, *27*, 1247–1252.
(37) Xie, Q.; Tang, Y.; Li, W.; Wang, X. H.; Qiu, Z. B. Investigation of the binding mode of (−)-meptazinol and bis-meptazinol derivatives on acetylcholinesterase using a molecular docking method. *J. Mol. Model.* **2006**, *12*, 390–397.
(38) Brunger, A. T. Assessment of phase accuracy by cross validation: the free *R* value. Methods and applications. *Acta Crystallogr., Sect. D: Biol. Crystallogr.* **1993**, *49*, 24–36.

JM801657V